Journal of Alloys and Compounds 637 (2015) 242–247

Contents lists available at ScienceDirect

Journal of Alloys and Compounds

journal homepage: www.elsevier.com/locate/jalcom

Influence of cooling rate on microstructure formation during rapid solidification of binary TiAl alloys

C. Kenel *, C. Leinenbach

Empa – Swiss Federal Laboratories for Materials Science and Technology, Überlandstrasse 129, 8600 Dübendorf, Switzerland

ARTICLE INFO

Article history:
Received 22 September 2014
Received in revised form 18 February 2015
Accepted 2 March 2015
Available online 9 March 2015

Keywords:
Intermetallics
Rapid-solidification
Microstructure
Phase transitions
Thermodynamic modeling
Computer simulations

ABSTRACT

Titanium aluminides as structural intermetallics are possible candidates for a potential weight reduction and increased performance of high temperature components. A method for the characterization of the microstructure formation in rapidly solidified alloys was developed and applied for binary Ti–(44–48)Al (at.%). The results show a strong dependency of the microstructure on the Al content at cooling rates between $6 \cdot 10^2$ and $1.5 \cdot 10^4$ K s^{-1}. The formation of $\alpha \rightarrow \alpha_2$ ordering, lamellar $\alpha_2 + \gamma$ colonies and interdendritic TiAl γ-phase were observed, depending on the Al amount. Based on thermodynamic calculations the observed microstructure can be explained using the CALPHAD approach taking into account the non-equilibrium conditions. The presented method provides a useful tool for alloy development for processing techniques involving rapid solidification with varying cooling rates.

1. Introduction

Titanium aluminides are structural intermetallics that are promising candidates for high temperature applications [1,2]. The binary Ti–Al phase diagram shows several intermetallic phases [3] (cf. Fig. 1). However, only the Ti_3Al α_2- and the TiAl γ-phases have been found to be of engineering importance. Furthermore, these two phases show the largest solubility range of intermetallic phases, whereas all other phases have rather limited solubility or are even line compounds. The range of technical alloys is restricted to the $\alpha_2 + \gamma$ phase field due to the formation of a lamellar structure leading to enhanced toughness. The alloy properties strongly depend on the phase morphology [2].

The emerging field of additive manufacturing (AM) requires alloys that are suitable for rapid solidification and subsequent cooling at small melt pool dimensions as well as multiple reheating and cooling cycles. Some attempts on the AM of titanium aluminide alloys have been reported recently [4–6]. While many experimental data are available regarding the phase evolution during solid state heat treatments and subsequent quenching [1,7–10], comparably little is known about microstructure formation during rapid solidification [11–14]. The Ti–Al system is well studied in the solid state up to cooling rates of 400 K s^{-1} [7,8]. However, the developed continuous cooling diagrams do not take into account the solidification step and established knowledge of rapid solidification is typically restricted to cooling rates above 10^5 K s^{-1}. Several studies using undercooled levitated alloys established the phase selection principles at high solidification speed and moderate cooling rates [15–18]. These studies rely on the absence of nucleation sites to achieve high undercooling, which is not realistic for AM. The AM of titanium aluminide alloys is still at its infancy for several reasons. First, titanium aluminides are inherently brittle at room temperature rendering them susceptible for severe cracking during processing due to thermal stresses. Second, many alloys have pronounced element segregation during casting [1], an effect that usually increases with a higher cooling rate. Furthermore, titanium aluminides undergo several solid state phase transformations. These transformations may be altered or completely suppressed at the typical cooling rates of 10^3–10^4 K s^{-1} of laser-based AM techniques and metastable phase relations can occur [11]. In this work, we systematically studied the microstructure and the phase evolution during rapid solidification of binary Ti–(44–48)Al (at.%) alloys at defined cooling rates between $6 \cdot 10^2$ and $1.5 \cdot 10^4$ K s^{-1}. For this, we developed a method which combines rapid solidification experiments of small alloy samples with finite element simulations of the temperature evolution in the samples and thermodynamic simulations using the CALPHAD method.

2. Materials and Methods

The Ti–(44–48)Al (at.%) master alloys for the rapid solidification experiments were produced by non-consumable tungsten electrode arc melting in water cooled Cu crucibles in 500 mbar Ar atmosphere, purified by an OXISORB cartridge

* Corresponding author. Tel.: +41 58 765 5654.
E-mail address: Christoph.Kenel@empa.ch (C. Kenel).

http://dx.doi.org/10.1016/j.jallcom.2015.03.016
0925-8388/

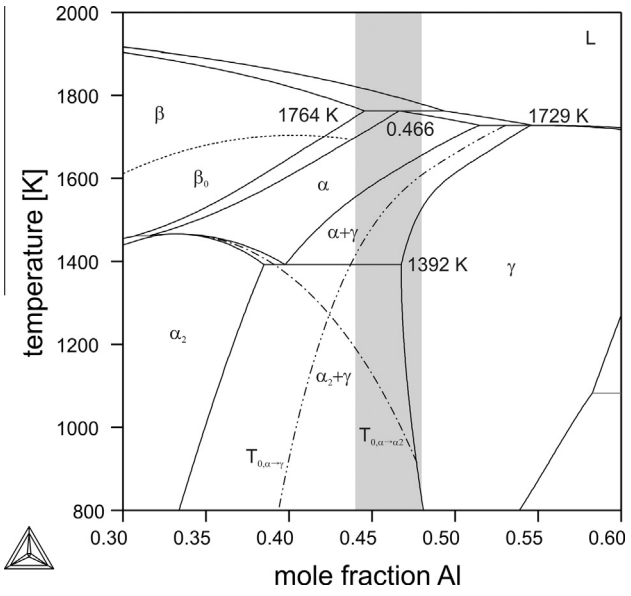

Fig. 1. Calculated binary Ti–(30–60)Al phase diagram based on [3]. Overlayed are the $T_{0,\alpha\rightarrow\alpha 2}$ (dot-dashed) and $T_{0,\alpha\rightarrow\gamma}$ (double dot-dashed) temperatures and the compositional range of the studied alloys (shaded).

(Messer). As starting materials Ti (99.98%) and Al (99.999%) from Alfa Aesar were used. Every alloy was re-melted eight times to ensure good sample homogeneity. No chemical analysis was performed because the material losses after arc melting were <0.3%. The rapid solidification experiments were performed by re-melting and rapid cooling of small samples (2–250 mg) of the master alloys under similar conditions as the initial alloy production. The electric arc was ignited directly above the prealloyed material and hold for approximately 1 s to melt the specimen. Then the arc was immediately moved at maximum distance from the specimen and allowed to cease to prevent overheating the specimen and alter the formed microstructure or reduce the cooling rate. Fig. 2a shows a schematic drawing for the rapid solidification experiment.

The cooling rate as a function of the specimen radius was estimated using finite element modeling using Abaqus/CAE 6.13-2 (3DS Simulia) with a 160,000 element hexahedral (DC3D8) mesh. The minimal mesh size was 1/50th of the specimen diameter. The specimen was assumed perfectly spherical with a radius r and a height of $1.8{\cdot}r$ (cf. Fig. 2b). The geometry was chosen based on measurements from real specimens. The water cooled Cu crucible was modeled only in the surrounding space as a simplified cylindrical Cu part (cf. Fig. 2c). The contact area in the simulation was assumed perfectly flat and horizontal. Direct contact was assumed between the specimen and the Cu crucible. In the areas of the Cu part close to the contact zone with the specimen a fine mesh was used in order to compute small time steps with high thermal gradients. Substrate areas in far distance from the specimen were meshed with larger sized elements to reduce computational cost (cf. Fig. 2c). The temperature of the Cu substrate was set to $T = 293$ K on the lower surface and the circumferential plane. The model included conductive heat transfer between the specimen and the Cu substrate as well as surface radiation from the specimen to the ambient surrounding. For Ti–Al published data of a Ti–Al–Nb alloy was used due to the large range in temperature and the completeness of the set of thermophysical properties [19]. For Cu, a thermal conductivity of 398 W m^{-1} K^{-1} at $T = 298$ K and 357 W m^{-1} K^{-1} at $T = 1000$ K, respectively, was set for the simulation [20]. During arc melting the water cooled Cu crucibles do not melt and thermophysical data for Cu is not needed for high temperatures or the liquid state.

A transient analysis of the temperature change with an initial temperature of the liquid alloy droplet of 2000 K was applied to extract the cooling curves at various positions of the specimen and to calculate the corresponding characteristic cooling rates $\left|\frac{\Delta T}{\Delta t}\right|_{T=1273K}$ at $T = 1273$ K. This temperature is below the eutectoid temperature ($T = 1392$ K) according to the binary Ti–Al phase diagram and is in the $\alpha_2 + \gamma$ two phase field (cf. Fig. 1). The initial temperature for transient heat transfer analysis was set based on pyrometer temperature measurements of the melt during arc melting of the master alloys. The results indicate that increased convection in the melt and very effective heat removal by the Cu crucibles avoids overheating the melt above 2000 K. Small specimens with low contact area and restricted convection may achieve higher temperatures. The temperature changes for the center and top point of the sphere were extracted from the finite element simulation and used for further analysis (cf. Fig. 3). The characteristic cooling rate

$$\left|\frac{\Delta T}{\Delta t}\right|_{T=1273K} = \frac{1}{2} * \left(\left|\frac{\Delta T}{\Delta t}\right|_{T=1273K,top} + \left|\frac{\Delta T}{\Delta t}\right|_{T=1273K,center}\right) \quad (1)$$

was defined as the mean slope $|\frac{\Delta T}{\Delta t}|$ at a temperature of $T = 1273$ K for the top and center position of the spherical specimen. Based on the finite element simulations a function correlating the specimen radius r and the characteristic cooling rate $\left|\frac{\Delta T}{\Delta t}\right|_{T=1273K}$ was derived according to

$$\left|\frac{\Delta T}{\Delta t}\right|_{T=1273K} = a \cdot r^{b} \quad (2)$$

The exponent $b = -2$ of the power law curve can be determined by a dimensional analysis. Based on the dependency of the cooling rate on the contact area A, specimen volume V and the distance to the interface to the Cu crucible d (cf. Fig. 2b). As $\frac{\Delta T}{\Delta t} \sim \frac{A}{dV}$; and $A \sim r^2$, $V \sim r^3$ and $d \sim r$; it follows that $\frac{\Delta T}{\Delta t} \sim r^{-2}$. The results of the simulations show that this idealized analysis is a valid assumption as the calculated values only slightly differ from the idealized curve based on

$$\left|\frac{\Delta T}{\Delta t}\right|_{T=1273K} = a \cdot r^{-2} \quad (3)$$

as can be seen in Fig. 4a. Thus, the entire curve can be described using a single material parameter $a = 4354 \pm 7 \cdot 10^{-6}$ K m^2 s^{-1} in a range of $0.5 \leqslant r \leqslant 2.5$ mm. The upper and lower boundaries correspond to the cooling rates at the top and center position of the specimen, respectively (cf. Fig. 4a). Considering the low bandwidth between both boundaries the upper hemisphere of the spherical specimens can be assumed to have similar thermal histories irrespective on the exact location.

The finite element simulations were verified by high-speed camera measurements using a Motion Xtra HG-100 K high-speed camera with an acquisition rate of 500 Hz and 200 µs dwell time. Considering a changing surface emissivity as a function of the temperature, the solidification front propagation can be monitored [21,22]. The measurements showed comparable solidus surface propagation in comparison with the simulation with a solidus temperature of 1773 K (cf. Fig. 4b). Due to geometrical restrictions of the arc furnace, the high-speed camera frames were taken from an inclined angle with respect to the upper substrate surface, which leads to a tilted view on the specimens (cf. Fig. 2a). Based on these measurements, the calculated cooling rates are assumed to be representative for the studied specimens.

The characteristic cooling rates $\left|\frac{\Delta T}{\Delta t}\right|_{T=1273K}$ were varied from $6 \cdot 10^2$ to $1.5 \cdot 10^4$ K s^{-1} by varying the sample radii in a range from 0.54 mm to 2.57 mm. For the microstructural analysis the specimens were embedded into epoxy resin and polished using diamond suspensions from 9 to 0.25 µm (MetaDi, Buehler). The final polished specimens were prepared using a 20 nm silica solution (MasterMet 2, Buehler) with H_2O_2 addition. The so-prepared specimens were investigated using optical microscopy (OM) using a Zeiss AXIOBSERVER under polarized light; by scanning electron microscopy using a Hitachi S3700N equipped with BSE and EDX detectors (EDAX); and with X-ray diffraction (XRD) with Cu Kα radiation using a Bruker D8 DISCOVER equipped with a LynxEye detector. Measurements

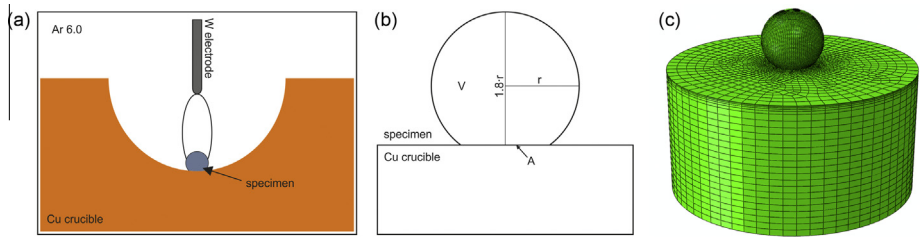

Fig. 2. (a) Schematic drawing for the geometrical situation for rapid solidification. The arc is ignited between the specimen and the tungsten electrode, while the water cooled Cu crucible acts as a heat sink; (b) Geometry of the specimen used for finite element simulations; (c) Meshed part with a fine mesh in the specimen and in the Cu substrate close to the contact area.